Water Research 91 (2016) 115–125

Contents lists available at ScienceDirect

Water Research

journal homepage: www.elsevier.com/locate/watres

Removal of aqueous nC_{60} fullerene from water by low pressure membrane filtration

R. Floris [a, b], K. Nijmeijer [b], E.R. Cornelissen [a, *]

[a] KWR Watercycle Research Institute, PO Box 1072, 3430 BB Nieuwegein, The Netherlands
[b] Membrane Science & Technology, University of Twente, Mesa+ Institute for Nanotechnology, PO Box 217, Enschede 7500 AE, The Netherlands

ARTICLE INFO

Article history:
Received 31 March 2015
Received in revised form
31 August 2015
Accepted 11 October 2015
Available online 23 October 2015

Keywords:
Membrane
Fullerene
Backwash
Nanoparticle filtration

ABSTRACT

The potential environmental and health risks of engineered nanoparticles such as buckminsterfullerene C_{60} in water require their removal during the production of drinking water. We present a study focusing on (i) the removal mechanism and (ii) the elucidation of the role of the membrane pore size during removal of nC_{60} fullerene nanoparticle suspensions in dead-end microfiltration and ultrafiltration mimicking separation in real industrial water treatment plants. Membranes were selected with pore sizes ranging from 18 nm to 500 nm to determine the significance of the nC_{60} to membrane pore size ratio and the adsorption affinity between nC_{60} and membrane material during filtration. Experiments were carried out with a dead-end bench-scale system operated at constant flux conditions including a hydraulic backwash cleaning procedure. nC_{60} nanoparticles can be efficiently removed by low pressure membrane technology with smaller and, unexpectedly, also by mostly similar or larger pores than the particle size, although the nC_{60} filtration behaviour appeared to be different. The nC_{60} size to membrane pore size ratio and the ratio of the cake-layer deposition resistance to the clean membrane resistance, both play an important role on the nC_{60} filtration behaviour and on the efficiency of the backwash procedure recovering the initial membrane filtration conditions. These results become specifically significant in the context of drinking water production, for which they provide relevant information for an accurate selection between membrane processes and operational parameters for the removal of nC_{60} in the drinking water treatment.

1. Introduction

The increasing use of engineered nanoparticles (eNPs) in consumer products like food, paints, coatings, cosmetics, personal care products, etc. (Benn et al., 2011; Murayama et al., 2004; Osawa, 2002) will lead to direct and indirect release of eNPs to the environment and to sources for drinking water. Specifically Buckminsterfullerene (C_{60}) (Kroto et al., 1985) has received a considerable amount of attention due to its particular chemical physical properties (Guldi and Prato, 2000) i.e. high hydrophobicity, heat resistance and superconductivity, which explains its wide spread use in different applications (Baena et al., 2002; Osawa, 2002). Although non derivatized C_{60} nanoparticles have a very low solubility in water (Heymann, 1996) and are highly hydrophobic ($K_{ow} = 6.67$ (Jafvert and Kulkarni, 2008)) C_{60} nanoparticles can form nano-sized colloidal aggregates in water (usually and here as well referred to as nC_{60}) (Deguchi et al., 2001) and could therefore end up in aquatic environments when released to the environment. Several studies reported C_{60} toxicity to various organisms (Chae et al., 2009; Lyon et al., 2006; Sayes et al., 2005; Song et al., 2012). These results are still under debate because it is not completely clear if the toxicity reported is related to the C_{60} itself or that the preparation method of nC_{60} colloidal suspensions as well influences the toxicological results (Zhu et al., 2006). However, due to this possible toxicological nature, the removal of nC_{60} from water becomes mandatory to ensure the production of safe drinking water and to minimize human exposure to eNPs via ingestion. Moreover, eNPs can serve as pollutant carriers (Hofmann and von der Kammer, 2009; Navarro et al., 2008; Stone et al., 2010) potentially resulting into inadequacy of existing treatment processes. This uncertainties on nC_{60} toxicity and the nC_{60} potentiality as pathogens carrier result in a mandatory removal of nC_{60} in water treatment plants. Low pressure membranes are a viable solution in removing contaminants that are similar in size to nNPs such as viruses, protozoa cysts

* Corresponding author.
E-mail address: emile.cornelissen@kwrwater.nl (E.R. Cornelissen).

http://dx.doi.org/10.1016/j.watres.2015.10.014
0043-1354/

(H. Guo et al., 2010a,b) and colloids (Schafer, 2000). Thus it is expected that eNPs can be effectively removed by low pressure membrane filtration as well. However so far, detailed studies on the effectiveness of the filtration for eNPs, their filtration behaviour and their exact removal mechanism are lacking.

Some studies focused on a single specific aspect related to interactions between eNPs and low pressure membranes have been carried out in different fields of membrane research, such as eNP characterization (Baalousha et al., 2011), eNP size separation (Akamatsu et al., 2010; Xie et al., 2009) and membrane integrity tests (H. Guo et al., 2010a,b), but to the best of our knowledge only very few studies dealt with the understanding of the removal mechanism of eNPs by membrane filtration techniques. Destabilized fullerene suspensions (nC_{60} and fullerol) were filtered through 20 nm ceramic membranes under variable ionic strength, ionic composition and pressure gradients (Jassby et al., 2010). The removal efficiency was below 80% at a transmembrane pressure of 20 kPa. The separation of fullerenes from the aqueous suspension increased, or decreased, depending on the solution pH and ionic strength, while transmembrane pressure only affected the retention of fullerol. The interactions between a set of functionalized eNPs and polymeric membranes composed of different materials and pore sizes (ranging from 2 nm to 200 nm) were investigated as well (Ladner et al., 2011). The authors observed in general (i) a dependency of the particle size to membrane pore size ratio on the removal efficiency and (ii) that removal mechanisms were influenced by the surface affinity between nanoparticles and membranes, facilitating also the removal of eNPs smaller in size than the membrane pores. They also concluded that the eNP properties appeared to be more important in determining the transport behaviour than the membrane properties. Although the aforementioned studies provided valuable knowledge on the interactions between eNPs and low pressure membranes, the results are difficult to translate to real water treatment plants because none of the reported studies (i) was performed under typical full-scale conditions such as a constant flux operating mode in dead-end membrane systems and (ii) used a hollow fiber membrane configuration typically used in water treatment plants (Crozes et al., 1997; Howe et al., 2007; Tarabara et al., 2002). To bridge this gap the focus of the present study is on (i) the removal mechanism of nC_{60} fullerene nanoparticles from suspensions in dead-end hollow fiber microfiltration and ultrafiltration and (ii) the elucidation of the role of membrane pore size on the removal and removal mechanisms of nC_{60} fullerene nanoparticles. To the best of our knowledge this work is the first one reporting nanoparticle filtration experiments performed under constant flux operating mode in dead-end membrane systems using commercially available hollow fiber membranes and including a backwash cleaning procedure with multiple cycles. Removal and removal mechanisms were evaluated by analysing transmembrane pressure (TMP) changes during filtration, measuring permeability recovery and performing membrane autopsy by visual and electron microscopy observation of the deposition of nC_{60} on the inner membrane surface.

2. Theory

Based on previous studies (Jassby et al., 2010; Ladner et al., 2011), particle size distribution is expected to play an important role in determining the removal efficiency and removal mechanism by low pressure membrane filtration. A high removal of nanoparticles by tight membranes (pore size smaller than nanoparticle diameter) is expected and size exclusion is expected to be the dominant separation mechanism, whereas for the more open membranes (pore size larger than nanoparticle diameter) a lower removal is expected, where removal is predominantly due to a combination of adsorption onto the membrane material and pore entrapment in the internal membrane structure. Removal can also occur when the membrane pore size is much larger than the nanoparticle diameter (Ladner et al., 2011) if membrane and nanoparticles have an adsorption affinity (Fig. 1c).

Retention can occur (a) by deposition onto the membrane surface resulting in external deposition (cake layer formation) and pore blocking (Fig. 1a: the pore size is smaller than the nanoparticles diameter), (b) by deposition into the membrane internal structure resulting in pore entrapment and pore narrowing (Fig. 1b: the pore size is larger than/comparable to the nanoparticle diameter) and (c) by adsorption onto the internal and external membrane surface due to nanoparticle and membrane adsorption affinity (Fig. 1c). Retention cannot occur if the membrane pore size is larger than the eNPs diameter and there is no adsorption affinity between eNPs and the membrane material (Fig. 1d).

Some eNPs accumulated on the membrane surface or in the

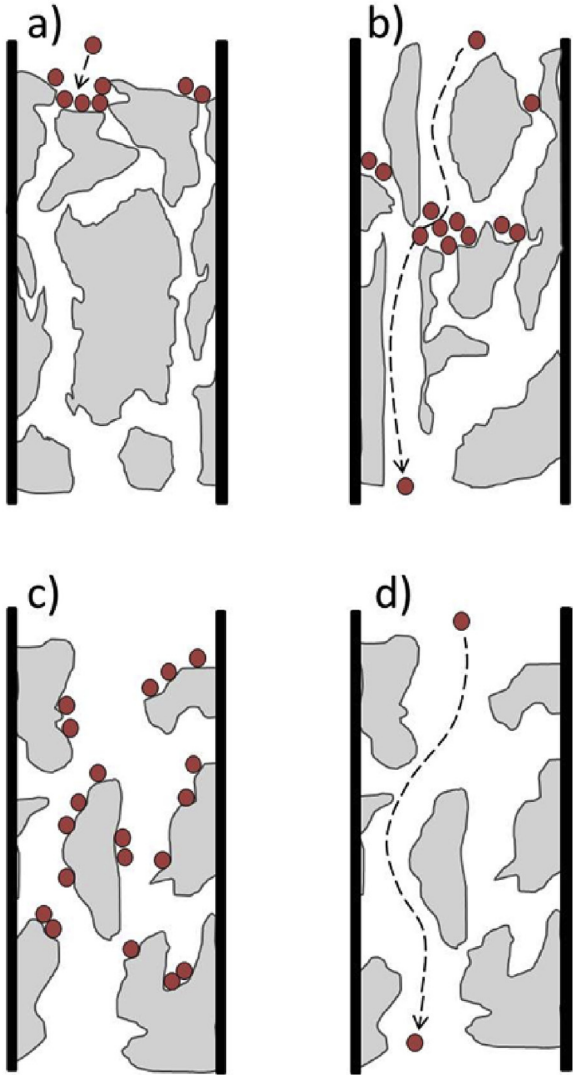

Fig. 1. Different nC_{60} removal mechanisms expected for low pressure membranes: a) Pore size smaller than nC_{60} size resulting in high removal efficiency and surface layer deposition combined with pore blocking; b) Pore size larger/comparable than nC_{60} size resulting in partial removal and internal membrane deposition (pore entrapment and pore narrowing); c) Pore size larger than nC_{60} size and adsorption affinity resulting in partial removal of eNPs; d) Pore size larger than nC_{60} size without adsorption affinity resulting in eNPs breakthrough (adapted from (Ladner et al., 2011)).

membrane structure may be removed by physical (or chemical) cleaning but some fouling, more likely fouling that deposit in the membrane structure might be irreversible (Fane et al., 2006). eNPs that deposit within the membrane pore structure are likely to be subjected to less substantial hydraulic shear forces, and may therefore not be effectively removed through physical actions like backwashing (Henry et al., 2012). Therefore we assume that a deposited cake-layer (Fig. 1a) can be removed by a hydraulic backwash sequence recovering the initial membrane permeability (Li et al., 2010; Mulder, 1991), while pore blockage, pore constriction and adsorption (Fig. 1b and c) will result in nC_{60} accumulation in the membrane structure in time resulting in an increase of the transmembrane pressure in time (Crozes et al., 1993; Huang et al., 2007; Singh, 2015).

The resistance in series model can be applied to identify differences in the particle deposition/removal mechanisms (Cho et al., 1999; Hong and Elimelech, 1997; Mulder, 1991). The flux in porous media can be described by Darcy's Law (Equation (1)):

$$J = \frac{TMP}{\nu \cdot R_{tot}} \quad (1)$$

Where J is the water flux [$L/m^2 \cdot h$], TMP is the transmembrane pressure [bar], ν is the dynamic viscosity of the feed solution [Pa·s], and R_T is the total hydraulic membrane resistance [1/m]. R_T can also be written as:

$$R_T = R_M + R_E + R_I \quad (2)$$

Where R_M is the hydraulic resistance of the clean membrane, R_E is the resistance due to the external cake-layer deposition (Fig. 1a) and R_I is the resistance due to internal pore blockage and pore constriction (Fig. 1b and c). All resistances are expressed in 1/m and can be obtained from the experimental data of a series of filtration and backwash cycles. Rearrangement of Equation (1) after substitution of Equation (2) in Equation (1) yields Equation (3):

$$R_T = \left|\frac{TMP}{\nu \cdot J}\right| \quad (3)$$

During filtration of ultrapure water through a virgin membrane, internal and external deposition of eNPs does not occur. Therefore $R_E = R_I = 0$ and only R_M contributes to the total hydraulic resistance, which can thus be calculated as follows:

$$R_M = \left|\frac{TMP}{\nu \cdot J}\right|_{virgin} \quad (4)$$

R_T is obtained from the nC_{60} filtration experiments considering the TMP at the end of the filtration cycle after both external and internal deposition:

$$R_T = \left|\frac{TMP}{\nu \cdot J}\right|_{fouled} \quad (5)$$

Experimental data on ultrapure water permeation through a fouled and backwashed membrane (assuming that external deposition is completely removed by hydraulic shear forces) allows the calculation of the remaining resistance:

$$R_I = \left|\frac{TMP}{\nu \cdot J}\right|_{backwashed} \quad (6)$$

Finally R_E can be obtained by rearranging Equation (2):

$$R_E = R_T - R_M - R_I \quad (7)$$

3. Material and methods

3.1. Reagents and chemicals

Fullurene-C_{60} (purity >99.5%) was obtained from Sigma Aldrich (Steinheim, Germany). Toluene was purchased from Mallinckrodt Baker B.V. (Deventer, The Netherlands). Ultrapure water (18.2 mΩ cm) was obtained by purifying demineralized water in a Milli-Q system (Millipore, Bedford, MA).

3.2. Preparation of aqueous fullerene suspensions

Stable aqueous nC_{60} nanoparticle suspensions were prepared using a solvent exchange/sonication procedure (Chen and Elimelech, 2007). Briefly, 50 mg of C_{60} fullerene powder was added to 100 mL toluene and was stirred for at least 12 h to achieve complete dissolution of the fullerenes. The C_{60} solution was added to 350 mL ultrapure water in a 600 mL beaker. Toluene was evaporated in a sonication bath (Branson) at an energy intensity of 125 W. Ultrapure water was regularly added each hour to compensate the volume loss due to toluene evaporation and to avoid fullerene deposition. The resulting colloidal suspension was finally filtered through a 0.45 and 0.22 μm cellulose acetate vacuum filter system (Corning Amsterdam, The Netherlands) resulting in a nC_{60} stock solution concentration of 15–20 mg/L. Prior to the filtration experiments the obtained stock solution was diluted in ultrapure water to obtain a membrane feed solution of 1.03 ± 0.17 mg/L.

3.3. Characterization of aqueous fullerene suspension size

Characterization of the nC_{60} feed suspension, permeate and backwash samples, was performed with a set of different analytical techniques. The formation of the colloidal suspensions was corroborated by a UV–vis spectrophotometer. Concentrations of nC_{60} suspensions were measured after liquid–liquid extraction by liquid chromatography coupled to high-resolution mass spectrometry and UV spectrophotometry (LC-MS-UV) (Kolkman et al., 2013). The size distribution was determined by dynamic light scattering (DLS), nanoparticle tracking analysis (NTA) and analytical ultra-centrifugation (AUC). DLS measurements were performed with a Zetasizer Nano-ZS (Malvern Instruments, Worcestershire, UK). Samples were measured at 25 °C, in triplicate, and each measurement was the average of at least 15 runs. NTA measurements were performed with a NanoSight LM10 (NanoSight, Amesbury, UK). Samples were diluted in order to reach the recommended measurement concentration of about 10^8 particles/mL (Filipe et al., 2010) which corresponds approximately to a nC_{60} concentration of 0.5 mg/L. The AUC measurements to determine the nC_{60} size distributions were made using a disc centrifuge (CPS Instruments Inc., USA). Measurements were made at a disc rotation speed of 20,000 rpm and particle sedimentation was carried out at a 8–24 wt % sucrose density gradient. Prior to each sample measurement the instrument was calibrated using PVC nanosphere standards (476 nm). Electrophoretic mobility measurements were used to evaluate the surface charge and zeta potential determined with a Zetasizer Nano-ZS (samples measured 6 times per measuring point).

3.4. Membrane and membrane characterization

To understand the role of membrane pore size on the membrane removal and removal mechanism, three low-pressure membranes differing in pore size were selected. Two microfiltration membranes (200 nm and 500 nm pore size) and one ultrafiltration

membrane (18 nm pore size and 150 kDa MWCO) were supplied by Pentair X-Flow (Enschede, The Netherlands). These were all commercially available hollow fiber polymeric polyethersulfone membranes containing polyvinylpyrrolidone that were operated inside-out. The commercial names of the membranes are reported in Table 1. Lab-scale membrane modules were prepared by potting membrane fibers with a two component epoxy resin (Polipox, Poliservice, Amsterdam, The Netherlands) in a transparent plastic tube (poly vinyl chloride) of 23 cm length and 1 cm diameter to obtain a membrane filtration area of 10 cm^2. The housing is equipped with a feed inlet connection (is also the backwash outlet connection), a permeate outlet connection (is also the backwash inlet connection) and two manually adjustable valves to release air bubbles that might form inside the fibers and/or the housing.

In this study membranes were characterized with respect to pore size, inner surface charge and pure water permeability. The pore size and pore size distribution of the membranes was measured with a Porolux 1000 capillary flow porometer (Porometer NV). Wetting fluid was used to wet the membrane prior to the measurements, which were carried out in duplicate. The mean pore diameter was calculated from the mean flow pressure, which corresponds to the intersection of the wet curve with the calculated half–dry curve (calculated from a dry and a wet run (Agarwal et al., 2012; Li et al., 2006)). The zeta potential of the inner surface of the membranes was measured using a SurPASS electrokinetic analyzer (Anton Paar GmbH). Measurements were carried out with 5 mM KCl as a background electrolyte solution. The pH was adjusted to values between 3 and 9.5 using aqueous 0.1 M NaOH and 0.1 M HCl solutions. The zeta potential was calculated according to the Fairbrother-Mastin equation (Ariza and Benavente, 2001). The membrane characteristics and module geometries are summarized in Table 1.

3.5. Membrane filtration apparatus and filtration procedure

Pure water flux and nC_{60} filtration measurements were performed with a lab-scale pilot (Fig. 2). A constant feed flow of 0.5 L/h was provided by a pulsation free neMESYS syringe pump (Cetoni GmbH, Germany) connected to the feed vessel. A pressure sensor in the feed line measured the transmembrane pressure (TMP) in front of the membrane every 5 s and an average TMP out of 3 measurements was logged every 15 s. A pressurized vessel (3 bars) containing fresh ultra-pure water combined with a flow controller was connected to a permeate line for the backwash sequence. A 20 s backwash occurred automatically every 20 min. The filtration measurement duration was 2 h resulting in a series of 6 filtration cycles and 6 backwash sequences. All these experiments were performed at a constant temperature of 20 °C. Feed and cumulative permeate samples were collected and analysed for rejection calculations. MF05 permeate samples were collected during filtration cycle number one, two, four and six to evaluate nanoparticle removal and nanoparticle size distribution at different filtration stages. After the last backwash procedure, the membrane was flushed with ultra-pure water to evaluate the membrane permeability after nanoparticle filtration, from which the pure water permeability recovery was calculated, which is an indirect indication of the particles remaining on the membrane after the cleaning procedure.

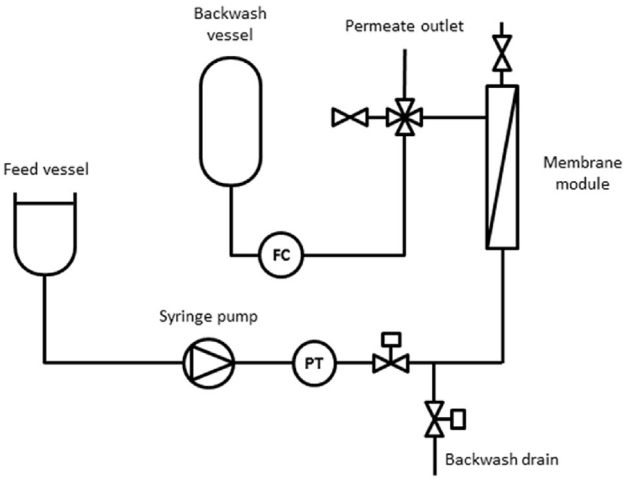

Fig. 2. Schematic representation of the lab-scale installation for constant flux filtration experiments.

3.6. Data handling

We evaluated the removal efficiency (R [%]) of nC_{60} dispersions as the nC_{60} rejection calculated from Equation (8):

$$R = \left(1 - \frac{C_p}{C_f}\right) \times 100 \quad (8)$$

Where C_p is the permeate concentration and C_f is the feed concentration [mg/L].

To assess the removal mechanism of nC_{60} by the low-pressure membranes, we analysed the evolution of measurable process parameters in time. The membrane permeability k [m/Pa·s] is defined as the reciprocal of the filtration resistance and can be calculated by Equation (9):

$$k = \frac{J}{TMP} \quad (9)$$

Where J is the water flux [L/m^2·h] and TMP is the transmembrane pressure [bar].

The subsequent permeability recovery is given by Equation (10):

Table 1
Membrane and module characteristics.

Commercial name	UFC M5	MF02 M2	MF05 M2
Membrane process	Ultrafiltration	Microfiltration	Microfiltration
Pore size* [nm]	18	200	500
Average pore size measured [nm]	15	186.6	745.6
Smallest pore size measured [nm]	-**	180.6	578
Filtration area [cm^2]	10	10	10
Fibers/module [-]	2	1	1
Inner fiber diameter [mm]	0.8	1.5	1.5
Volume/Area ratio [mm]	0.2	0.4	0.4
Zeta potential*** [mV]	−29.7 ± 4.5	−19.8 ± 5.1	−18.9 ± 7.7

* provided by manufacturer; ** not measured; *** measured at pH 6.5.

$$k_R = \frac{k_{After\ backwash}}{k_{Before\ filtration}} \times 100 \quad (10)$$

3.7. Application of pore blocking law for constant flux filtration

To clarify the removal mechanism occurring during UF18 and MF02 filtration blocking laws for constant flux low pressure membrane filtration were applied (Huang et al., 2008). Depending on the pore blocking mechanism the TMP increase during filtration can be described by

$$\frac{dTMP}{dV_s} = k_v(TMP)^n \quad (11)$$

Where Vs (m^3/m^2 or L/m^2) is the permeate throughput defined as the cumulative volume of permeate per unit of membrane area and k_v and n are 2 experimental parameters where n is a dimensionless number that is related to the pore blocking mechanism and k_v is related to the blocking mechanism and to the foulant concentration in the filtered water. The model has been applied here in the linearized form proposed by Huang e t al. (2008). The expressions and the coefficient are reported in Table 5 (Huang et al., 2008). For a more detailed explanation of the derivation we refer to the original publication (Huang et al., 2008).

4. Results and discussion

4.1. Characterization of nC_{60} suspensions

The nC_{60} UV/VIS absorption spectrum of the feed solution displayed two typical peaks at 250 and 360 nm, which is similar to previously reported results (Jung et al., 2013). The feed solution concentration was measured as 1.03 ± 0.17 mg/L. The size distributions obtained by DLS, NTA and AUC are reported in Fig. 3.

Similar and almost mono-modal asymmetric distributions were obtained. Next to the three different size distributions Fig. 3 also reports the mean particle size. The three size characterization techniques showed comparable results considering that these are based on different principles and measure different quantities: DLS measures the variation in intensity of scattered light, AUC determines UV adsorption by particles after separation in a concentration gradient, and NTA tracks (fluorescent) particles. For DLS, the distribution of the intensity is weighted based on the scattering intensity of each particle, which is proportional to the sixth power of the particle radius. This explains the presence of larger particles in the distribution (Fig. 3a). Despite of the differences in the size ranges detected by the different techniques, the size distributions show rather similar average values (Fig. 3). NTA measurements indicate a bimodal size distribution (Fig. 3b) which is most likely due to an artefact of the applied model used to interpret the NTA data or a consequence of the limited number of frames per particle analysed (Montes-Burgos et al., 2010). DLS is known to be problematic in detecting multimodal distributions (Dieckmann et al., 2009). However the second peak is not detected by AUC (Fig. 3c) whereas this is the only technique performing a sample fractionation during the measurements. AUC has higher resolution and accuracy compared to DLS and NTA (Anderson et al., 2013) and this supports the hypothesis of an artefact in the NTA size distribution. All size distributions obtained indicate that there is no overlap between the eNP size and the pore size of the UF18 and MF05 membranes. An overlap exists between particle size and pore diameter in case of the MF02 membrane. The largest sizes detected by NTA and AUC are in the range of 200–228 nm overlapping the MF02 membrane pore sizes. Despite of the small relative amount (2% and 0.4% respectively) this can play a role in the removal and removal mechanism of nC_{60}, as discussed later in this paper.

Table 2
Water permeability and corresponding resistance calculated according to Equations (9) and (4) respectively.

	UF18	MF02	MF05
Permeability (10^3 L/m^2·hour·bar)	0.87 ± 0.07	5.05 ± 0.45	8.3 ± 0.19
Membrane resistance (10^{11} 1/m)	4.3	0.7	0.5

Table 3
Membrane rejection of nC_{60}.

Membrane	UF18	MF02	MF05
Pore Size [nm]	18	200	500
Rejection [%]	99	99	10

Table 4
Surface tensions components and free energy of adhesion calculation.

	γ^{LW} (mJ/m^2)	γ^+ (mJ/m^2)	γ^{-+} (mJ/m^2)	ΔG_{MWS} (mJ/m^2)
Water	21.8	25.5	25.5	
Fullerenes*	43.16	0.61	1.66	
PES**	43	0.5	0.1	−80.259
PVP***	43	0	29.7	−41.751

* data obtained from (Henry and Brant, 2012); ** data obtained from (Cornelissen and Strathmann, 1998); *** data obtained from (Oss, 2006).

Table 5
Clean membrane and total hydraulic resistance calculated according to Equations (4) and (5) respectively.

	UF18	MF02	MF05
Clean membrane resistance (10^{11} 1/m)	4.3	0.7	0.5
Total hydraulic resistance (10^{11} 1/m)	4.4	1.1	0.5

4.2. Clean water flux measurements

Prior to each experiment milli-Q water was filtered at 0.5 L/h for at least 1 h or until a constant TMP was achieved to evaluate the clean water permeability of the membranes. When a constant TMP was not reached after 2 h of filtration the membrane module was discarded and replaced with a new one. Table 2 shows the clean water permeability for all 3 different membranes at a constant feed water flux together with the membrane resistance, calculated by Equations (9) and (4) respectively. Differences in values between the 3 membranes are the result of variations in several membrane morphological parameters such as porosity, tortuosity and pore interconnections (Alspach et al., 2008). The permeability values are within the typical range for UF and MF membranes (Mulder, 1991). These values will be used for the permeability recovery calculation of each membrane and to verify the stability and integrity of each membrane module.

4.3. Removal efficiency

The removal efficiency was observed to be dependent of the membrane pore size (Table 3).

The tight membrane (UF18) with pore sizes smaller than the nanoparticle diameter removed more than 99% of the nC_{60} suspended in water. As the minimum nC_{60} size determined was larger than the membrane pore size, the main removal mechanism is size

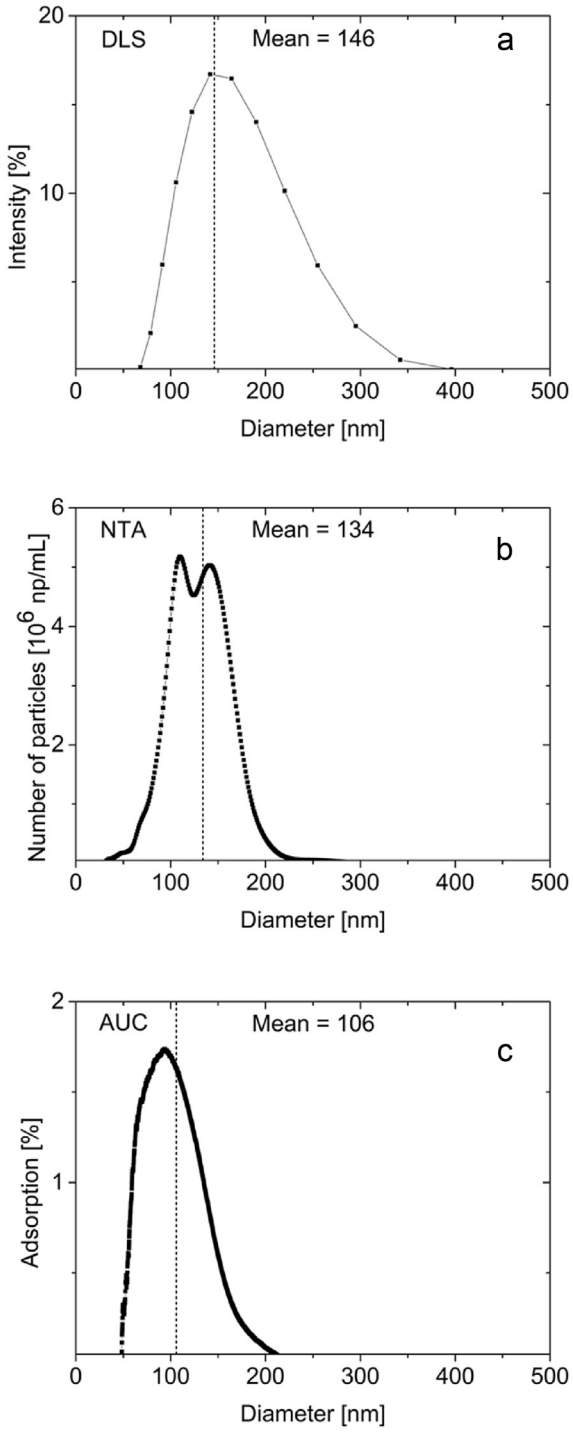

Fig. 3. nC_{60} size distributions with mean values (dashed lines): a) Intensity by DLS; b) Number of particles by NTA; c) Adsorption by AUC.

exclusion, as expected from the theoretical framework (Fig. 1a). However small amounts of nC_{60} were detected in the permeate samples (~8 μg/L). This can be attributed to an overlap between the membrane pore size and the nC_{60} size distribution, which could not be identified by our measurements. Another explanation was the existence of (i) nanoparticle clusters smaller than 18 nm or (ii) membrane pore sizes larger than the smallest eNPs cluster size measured (25 nm by NTA and 50 nm by DLS and AUC) occur. Another explanation if cluster-squeezing or partial cluster disaggregation due to the pressure gradient applied to the membrane interface (Jassby et al., 2010). The obtained removal efficiency was about 20% higher than the values reported in literature with similar membrane pore sizes (Jassby et al., 2010). This difference is hard to explain because detailed characterization of the ceramic membrane used by Jassby et al. is lacking. Furthermore, differences exist in the applied experimental conditions (e.g.: initial feed concentration, suspension volume filtered, filtration operation system, analytical method). The authors attributed the non-complete removal of nC_{60} to an overlap between the particle size distribution and the membrane pore size revealed by intensity-weighted PSD measurements of nC_{60} suspensions.

High removal (99%) of nC_{60} was also observed for MF02 despite the fact that the membrane pore size is predominantly larger than the size of nC_{60}. In this case, the smaller clusters of nC_{60} particles are expected to penetrate the membrane structure and either deposit on it or permeate through (Fig. 1b), whereas larger clusters of nC_{60} particles most likely deposit on the membrane surface either blocking or narrowing the membrane pores. The removal mechanism can be attributed to a combination of external deposition on and internal deposition in the membrane as will be further discussed in the membrane autopsy section. Removal results can also be affected by the duration of the experiments: longer filtration times could lead to a complete saturation of the membrane internal deposition volume available leading to a subsequent nC_{60} breakthrough. We could not observe this within the time frame of 6 cycles. The complete saturation of the internal membrane volume available for internal deposition can be expected after approximately 37 filtration cycles following a linear regression of the permeability recovery of MF02 in time (Fig. 5, discussed later) assuming that the permeability linearly decreases as filtration continues. As expected, the MF05 membrane showed a low nC_{60} removal of 10%, which can be explained from the removal scenario indicated in Fig. 1c. Free energy of adhesion calculations were performed using the Young–Dupré equation using surface tension components obtained from literature (Table 4). Calculations resulted in negative values for both polymers (PES and PVP) (Table 4) indicating that adhesion between nC_{60} and the membrane material is expected.

Possible fractionation effects on the eNP size distribution during filtration were investigated by comparing the feed size distribution with the permeate size distribution. Due to the low nC_{60} concentration in the UF18 and MF02 permeate samples the analysis was

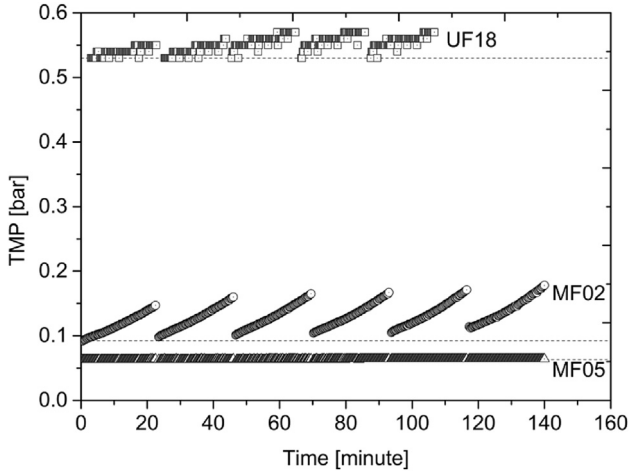

Fig. 4. Increase of the feed pressure due to nC_{60} deposition. Dashed line represents initial feed pressure.

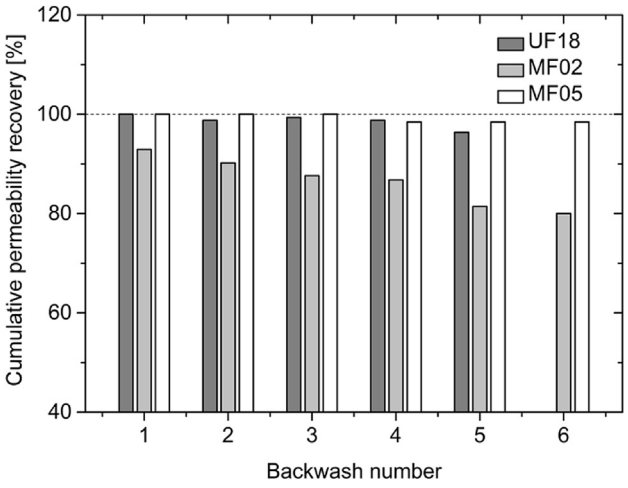

Fig. 5. Cumulative permeability recovery versus number of backwash cycles.

only conducted for the MF05 permeate samples and samples were analysed by DLS only. Permeate samples collected during filtration cycle number one, two, four and six showed the same average and polydispersity index values as the feed size distribution. This indicated that each size fraction is rejected at the same degree (10%).

4.4. TMP and permeability recovery (backwash efficiency)

During filtration when nC_{60} is retained by the membrane, the filtration resistance increases in time resulting in an increase in TMP during filtration at constant flux. The typical effect of nC_{60} deposition on TMP during 6 filtration cycles (5 filtration cycles for the UF18 membrane) and 6 backwash cycles is presented in Fig. 4. During constant flux filtration, the TMP increases due to the retention of nC_{60} and its deposition on and in the membrane for the UF18 and the MF02 membrane. Differences in initial TMP values for the 3 different membranes (see pure water flux section) are caused by differences in the membrane resistance due to differences in membrane porosity and membrane pore structure. During UF18 filtration the TMP increase per cycle is 31 ± 6 mbar on average and after the backwash procedure the initial TMP is almost completely restored (Fig 5). For the MF02 membrane, the TMP increase per cycle is 59 ± 8 mbar on average, but the initial TMP was not restored after backwash cleaning (Fig 5). The initial TMP before each filtration cycle kept increasing suggesting the occurrence of internal particle deposition (Lohwacharin and Takizawa, 2009). After each filtration cycle, the initial permeability of the UF18 membrane is recovered by the backwash up to 99 ± 1% (Fig 5). In contrast, the permeability recovery of the MF02 membrane showed a decreasing trend between the first and the last cycle from 93% to 81% (Fig. 5). This indicates the occurrence of pore entrapment and/or pore narrowing (Lohwacharin and Takizawa, 2009) (Fig. 1 b). The deposition of nC_{60} on MF05 did not significantly affect the TMP pressure during the experiments (1 mbar increase over 6 filtration cycles) and consequently the effect of the backwash procedure on the initial permeability was not observed. The evolution of permeability recovery following backwash cleaning highlights the differences in the removal mechanisms between UF18 and MF02 membranes. Although both membranes obtained the same high removal value, the MF02 membrane is more susceptible to pore entrapment and pore narrowing (internal deposition).

4.5. Membrane autopsy and SEM photos

The visual effects of the deposition of nC_{60} on the inner membrane surface after 6 filtration cycles and backwash cycles (5 filtration cycles for the UF18 membrane) are presented in Fig. 6. The lumen surface of the 3 membranes after nC_{60} filtration was visually very different. Although the initial membrane permeability was efficiently recovered after 5 backwash cycles, the inner membrane surface of the UF18 membrane was covered by a homogeneous dark brownish/blackish deposition layer consisting of nC_{60} (Fig. 6a). Some chunks of the deposition layer were removed, which can be visually observed in Fig. 6 by the lighter shades in the deposited black layer as indicated by white circles. A light brownish–yellowish more irregular deposition was observed for the MF02 membrane (Fig. 6b). Hardly any deposition was observed for the MF05 membrane (Fig. 6c), probably linked to the low nanoparticle removal. Changes in colour of the UF18 deposition layers can also be an indication of changes in the nC_{60} stability. Particles not removed from the membrane surface during the backwash procedure will increase the cake layer thickness and experience an increasing pressure difference, eventually giving rise to compression effects of the deposition layer (Braus et al., 2002). Deposition layer compression can ultimately bring eNPs beyond the energy barrier distance compromising their colloidal stability (Tang et al., 2011; Yiantsios and Karabelas, 1998). It has been shown that changes in size, structure, and/or interactions between the colloidal particles and solvent molecules can lead to colour changes (Gallagher et al., 1995) and this can also be the case of the changes in colours of the particle deposition layer observed here. More research is needed to clarify whether the fullerene on the deposition layer is still in colloidal state or solid precipitate. Differences in the physical status of fullerene can result in different degree of compaction of the deposition layer, which can affect both membrane performance (permeability decrease and nC_{60} removal) and the efficiency of the backwash cleaning procedure.

SEM photos of the internal membrane surfaces are presented in Fig. 7.

The inner/bore side surface of the UF18 hollow fiber membranes was covered by a compact deposition layer (Fig. 7a) with a thickness ranging from 1 to 6 μm (Fig. 7b). This is in agreement with the stipulation that during the filtration experiments particles are not removed by the backwash procedure, instead they accumulate on the membrane surface. Residuals of a deposited cake layer

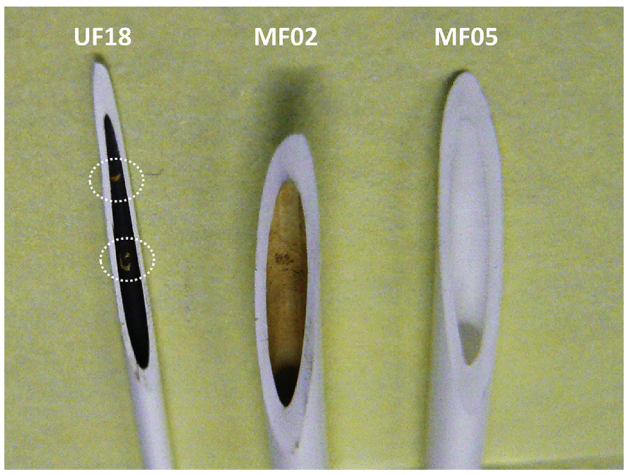

Fig. 6. Autopsy photo of UF18, MF02 and MF05 after 6 filtration and backwash cycles (5 for the UF18 membrane).

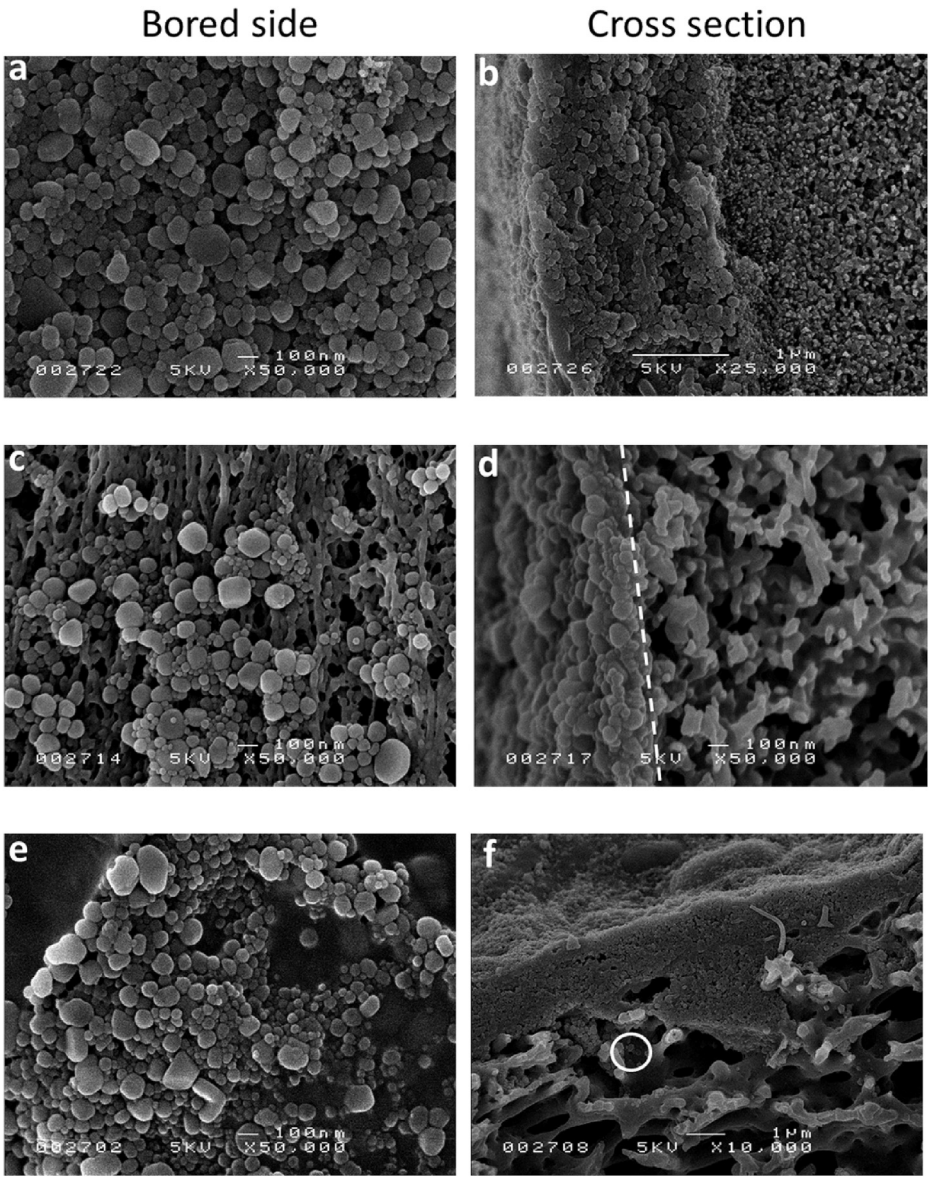

Fig. 7. SEM images of fouled membranes after 6 filtration and backwash cycles (5 for the UF18 membrane): a) UF18 bore side; b) UF18 cross section; c) MF02 bore side; d) MF02 cross section; e) MF05 bore side; f) MF05 cross section.

appeared also on the bore side surface of the MF02 membrane. However the inner/bore side surface was not fully covered (Fig. 7c). If a cake-layer was observed on the SEM picture the thickness of the layer deposited was about 100 nm (Fig. 7d). As expected, removal mainly occurred by external surface deposition visible as a cake layer and pore blocking instead of internal deposition. This resulted in a severe permeability loss as shown in Fig. 5. Surface deposition was also observed on the bore side MF05 membrane surface as a consequence of 10% removal of nC_{60} from the feed water. Regarding the MF05 the deposition was identified only on the feed side. The permeate side of the membrane appeared clean (image not shown here) in spite the presence of nC_{60} on the back wash water due to incomplete retention of the nanoparticles. Particle deposition seems to be localized into the valleys of the rough surface structure (Fig. 7e and f). If adhesion was occurring both at the feed and permeate side, the membrane would be (partially) covered by a nC_{60} deposition layer on both sides. Since this was not observed from the autopsy study using SEM, adhesion between nC_{60} and the membrane material is not expected to be the mechanism to responsible for 10% nC_{60} removal with the MF05 membrane. Most likely the adhesion effects are overshadowed by electrostatic repulsion effects between the negatively charged membranes (Table 1) and negatively charged nC_{60} (-79.3 ± 10.9 mV). Thus the 10% removal is attributed to surface deposition mainly occurring due to the roughness of the membrane surface (Fig. 7f). Deposition in the internal membrane structure has been identified by SEM analysis (white circle in Fig. 7f) in lower amounts than the surface deposition thought we exclude sorption phenomena due to nC_{60} and membrane interfacial affinity. This is in accordance with removal efficiency results discussed previously in Section 4.3. Differences in ratio of the cake-layer deposition resistance to the clean membrane resistance between the UF18 and MF02 explain the differences in the efficiency of removing the nC_{60} surface deposition by the backwash procedure. Resistance values (Table 5) were calculated by the resistance in series model (Cho et al., 1999; Hong and Elimelech, 1997).

In the case of the UF18 it was calculated that the hydraulic resistance of the deposition layer was one order of a magnitude lower than the clean membrane resistance. In these conditions the membrane structure dissipates most of the hydraulic shear stresses generated by the backwash flux. This results in a lower amount of energy available for the removal of the deposited cake layer compared to the MF02 membrane. Fig. 9 shows the ratio of the cake-layer deposition resistance to the clean membrane resistance versus the backwash cycle for the UF18 and the MF02 membranes. The contribution of the external deposition to the total filtration resistance in case of the UF18 was only ~5% (on average) with a very small variation within the 5 filtration cycles (±1.4%). In contrast, the contribution of the external deposition to the total filtration resistance in case of the MF02 membrane was ~26% during the first filtration cycle and stabilized in the following cycles at ~44 ± 1.6%. Moreover the presence of removed chunks (lighter colour of deposited black layer as indicated by white circles in Fig. 6) in the UF18 deposited cake-layer might eventually act as preferential flow pathways for the backwash flux reducing the potential cleaning effect of the backwash procedure. Similarly the formation of fractures in the deposition layer itself as shown in Fig. 8 can lead as well to preferential flow paths. However the fractures in Fig. 8 can also be the results of the sample drying preparation procedure for the SEM.

4.6. Application of the blocking laws for constant flux low pressure membrane filtration

Given the ratio of eNPs and membrane pore size we applied the intermediate blocking and cake formation model to the UF18 and MF02 membrane (see Section 3.7). The modelling and experimental results are presented in Fig. 10 for the first filtration cycle. The sum of squared residual values (S) (sum of squared deviations of predicted from experimental values of data) are reported in Table 6. S was adopted as a measure of the discrepancy between the experimental data and the model results.

Regarding the UF18 membrane the specific flux values from the experimental data corresponds closely (S = 0.14 ± 0.08) (Fig. 10) to the cake formation blocking law. Although this result does not exclude that other removal and fouling mechanisms are occurring, it confirm that deposition on the membrane surface is the major removal and fouling mechanism occurring in the ultrafiltration membrane.

Regarding the MF02 membrane, the experimental specific flux decrease fall between the calculated flux decrease of the 2 blocking laws (Fig. 10). It is therefore suggested that for the MF02 membrane both the cake formation and intermediate blocking mechanism are occurring at the same time.

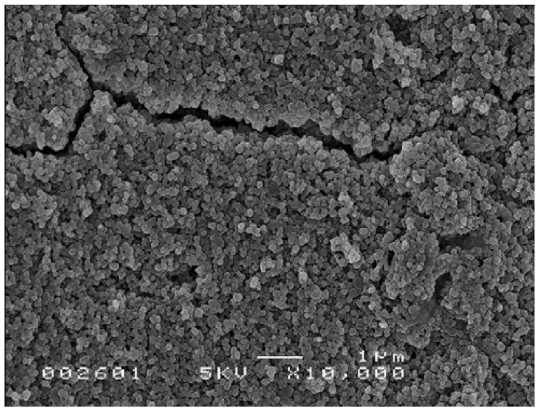

Fig. 8. SEM photo of fractured deposition layer on UF18 membrane.

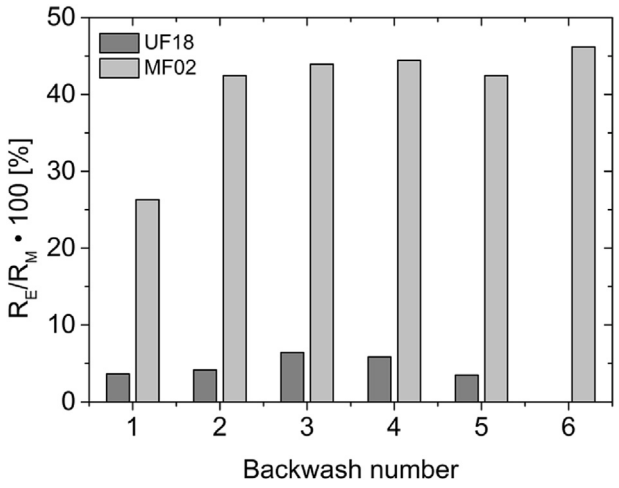

Fig. 9. Ratio of cake layer deposition resistance to clean membrane resistance versus number of backwash cycles.

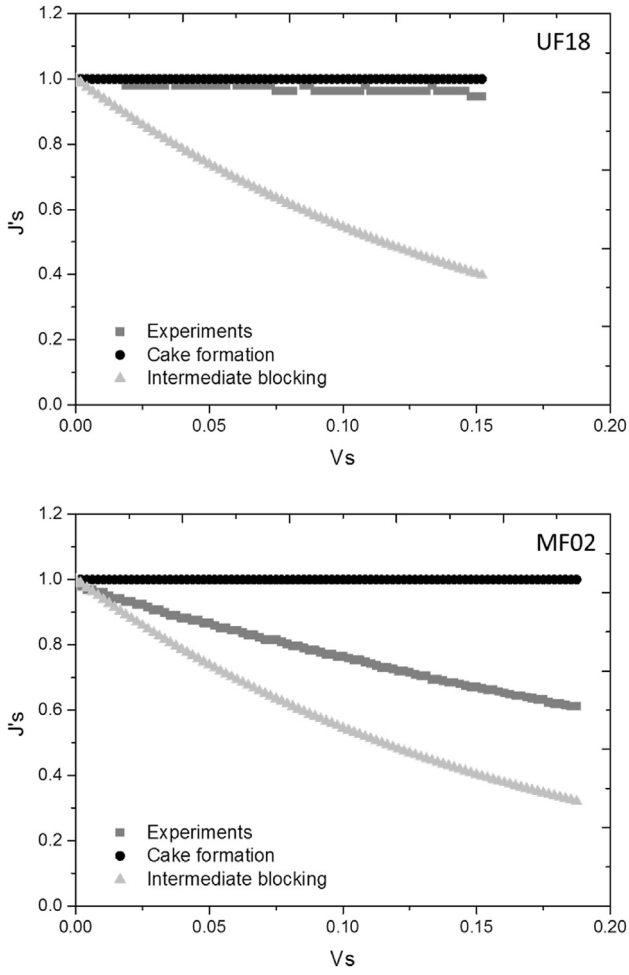

Fig. 10. Specific flux as function of the specific permeate volume for the experimental data, cake formation and intermediate pore blocking models relative to the first filtration cycle.

Table 6
The sum of squared residual values for the 2 membrane types and the filtration cycles.

	Cycle number						
Membrane	Blocking law	1	2	3	4	5	6
UF18	Cake formation	0.1	0.1	0.2	0.2	0.2	
	Intermediate blocking	9.6	9.6	8.5	8.4	8.6	
MF02	Cake formation	5.4	5.4	5.3	4.8	5.0	4.1
	Intermediate blocking	3.8	3.9	3.9	4.3	4.1	5.1

4.7. Discussion overall filtration behaviour under typical full-scale conditions

nC_{60} nanoparticles suspended in ultrapure water was efficiently removed by low-pressure membranes with an average pore size smaller and, unexpectedly, also by membranes with similar/larger than the particle size distribution. Much larger membrane pore size failed in retaining the nC_{60} nanoparticles. Membranes with pore size smaller than nC_{60} diameter removed more than 99% reaching efficiency considerably higher than previous studies (Jassby et al., 2010) reported. Even though small amounts of nC_{60} were detected in the permeate samples. During 5 filtration cycles each followed by a hydraulic backwash, the initial permeability was almost completely recovered. Nevertheless the majority of the deposition layer was still attached to the membrane surface at the end of the experiments. Visual observations suggest that colloidal stability of the nC_{60} might be compromised during the continuous accumulation of nC_{60}. Filtration by membranes with pore sizes mostly larger than nC_{60} size showed an unexpected removal of 99% which occurred by external surface deposition instead of internal deposition as expected. The backwash procedure was more effective in removing the deposition cake-layer but failed in recovering the initial filtration conditions resulting in a severe permeability loss. The ratio nC_{60} size to membrane pore size played an important role on the removal mechanism and on the efficiency of the hydraulic backwash procedure to recover the initial membrane filtration conditions. The efficiency of the hydraulic backwash procedure recovering the initial membrane filtration conditions was found also dependent on the ratio of the cake-layer deposition resistance to the clean membrane resistance. Moreover the efficiency of the cleaning procedure ultimately compromised the colloidal stability of the nC_{60} dispersion. The very low removal obtained by much larger membrane pore size (500 nm) mainly occurred by deposition on the rough membrane structure. We observed no particularly relevant adsorption phenomena between the nC_{60} and the membrane material. However, differently from previous work (Ladner et al., 2011) in this study the membrane surface proprieties played an important role in controlling the filtration behaviour of eNPs as well as their stability.

5. Conclusion

The effect of membrane pore size on the removal and on the removal mechanism of nC_{60} by low pressure membrane filtration including multiple backwash cycles was addressed. Multiple filtration and backwash cycles gave relevant insight in the filtration behaviour of nC_{60} with low pressure membranes. Commercially available low pressure membranes efficiently removed nC_{60} under typical full-scale conditions (i.e. constant flux operating mode in dead-end membrane systems). Water treatment plants which include low pressure membrane processes are a viable barrier in minimizing human exposure to nC_{60} via ingestion. However the membrane permeability during filtration and the efficiency of the backwash cleaning procedure can be strongly influenced by the ratio nC_{60} size to membrane pore size. These results become particularly significant in the context of the drinking water production, they give relevant information for an accurate selection between membrane processes and operational parameters for the removal of nC_{60} in the drinking water treatment. The work presented here provides systematic fundamental insights on the specific interactions of nC_{60} and the membranes and forms an essential understanding basis for future researches that include the use of natural waters. Further investigation is recommended to validate these findings in more environmentally relevant conditions addressing the role of water quality parameters on the filtration behaviour of nC_{60}.

Acknowledgement

This work is supported by NanoNextNL, a micro and nanotechnology consortium of the Government of The Netherlands and 130 partners. For the nanoparticle size distribution analysis, this research received also support from the QualityNano Project which is financed by the European Community Research Infrastructures under the FP7 Capacities Programme (Grant No. INFRA-2010-262163) and its partner University College Dublin. The authors would also like to acknowledge Marco Monopoli and Eugene Mahon (University College of Dublin) for the support in the nanoparticles size measurements, Herman Teunis (European Membrane Institute Twente) for the SEM analysis, Jens Potreck (Pentair X-Flow) for providing the membranes and Erik Emke (KWR Watercycle Research Institute) for the nanoparticle concentration analysis. The authors would specially like to thank Harry van Wegen and Sydney Meijering for building the installation set-up and their infinite help in developing the set-up.

References

Agarwal, C., Pandey, A.K., Das, S., Sharma, M.K., Pattyn, D., Ares, P., Goswami, A., 2012. Neck-size distributions of through-pores in polymer membranes. J. Memb. Sci. 415–416, 608–615.
Akamatsu, K., Han, F., Kaneko, Y., Nakao, S., 2010. Crossflow ultrafiltration properties of monodisperse nanoparticle suspensions in laminar flow. J. Chem. Eng. Jpn. 43, 938–945.
Alspach, B., Adham, S., Cooke, T., Delphos, P., Garcia-Aleman, J., Jacangelo, J., Karimi, A., Pressman, J., Schaefer, J., Sethi, S., 2008. Microfiltration and ultrafiltration membranes for drinking water. J. Am. Water Work. Assoc. 100, 84–97.
Anderson, W., Kozak, D., Coleman, V.A., Jämting, Å.K., Trau, M., 2013. A comparative study of submicron particle sizing platforms : accuracy, precision and resolution analysis of polydisperse particle size distributions. J. Colloid Interface Sci. 405, 322–330.
Ariza, M.J., Benavente, J., 2001. Streaming potential along the surface of polysulfone membrane: a comparative study between two different experimental systems and determination of electrokinetic and adsorption parameters. J. Memb. Sci. 190, 119–132.
Baalousha, M., Stolpe, B., Lead, J.R., 2011. Flow field-flow fractionation for the analysis and characterization of natural colloids and manufactured nanoparticles in environmental systems: a critical review. J. Chromatogr. 1218, 4078–4103.
Baena, J.R., Gallego, M., Valca, M., Division, A.C., 2002. Fullerenes in the analytical sciences. Trends Anal. Chem. 21, 187–198.
Benn, T.M., Westerhoff, P., Herckes, P., 2011. Detection of fullerenes (C60 and C70) in commercial cosmetics. Environ. Pollut. 159, 1334–1342.
Braus, E., Van Hoof, E., Molenberghs, B., Dotremont, C., Doyen, W., Leysen, R., 2002. A new method of measuring and presenting the membrane fouling potential. Desalination 150, 31–43.
Chae, S.-R., Wang, S., Hendren, Z., Wiesner, M., Watanabe, Y., Gunsch, C., 2009. Effects of fullerene nanoparticles on Escherichia coli K12 respiratory activity in aqueous suspension and potential use for membrane biofouling control. J. Memb. Sci. 329, 68–74.
Chen, K.L., Elimelech, M., 2007. Influence of humic acid on the aggregation kinetics of fullerene (C60) nanoparticles in monovalent and divalent electrolyte solutions. J. Colloid Interface Sci. 309, 126–134.
Cho, J., Amy, G., Pellegrino, J., 1999. Membrane filtration of natural organic matter: initial comparison of rejection and flux decline characteristics with ultrafiltration and nanofiltration. Water Res. 33, 2517–2526.
Cornelissen, E.R., Strathmann, H., 1998. Physicochemical aspects of polymer selection for ultrafiltration and microfiltration membranes. Colloids Surfaces A

Physicochem. Eng. Asp. 138, 283–289.
Crozes, G., Anselme, C., Mallevialle, J., 1993. Effect of adsorption of organic matter on fouling of ultrafiltration membranes. J. Memb. Sci. 84, 61–77.
Crozes, G.F., Jacangelo, J.G., Anselme, C., La, J.M., 1997. Impact of ultrafiltration operating conditions on membrane irreversible fouling. J. Memb. Sci. 124, 63–76.
Deguchi, S., Alargova, R.G., Tsujii, K., 2001. Stable dispersions of fullerenes, C 60 and C 70, in water. Preparation and characterization. Langmuir 17, 6013–6017.
Dieckmann, Y., Colfen, H., Hofmann, H., Petri-fink, A., 2009. Particle size distribution measurements of manganese-doped ZnS nanoparticles. Anal. Chem. 81, 3889–3895.
Fane, A.G., Xi, W., Rong, W., 2006. Interface Science in Drinking Water Treatment – Theory and Application, Interface Science and Technology. Elsevier.
Filipe, V., Hawe, A., Jiskoot, W., 2010. Critical evaluation of nanoparticle tracking analysis (NTA) by NanoSight for the measurement of nanoparticles and protein aggregates. Pharm. Res. 27, 796–810.
Gallagher, S.H., Armstrong, R.S., Lay, P.A., Reed, C., 1995. Solvent effects on the electronic spectrum of C60. J. Phys. Chem. 99, 5817–5825.
Guldi, D., Prato, M., 2000. Excited-state properties of C60 fullerene derivatives. Acc. Chem. Res. 33, 695–703.
Guo, H., Wyart, Y., Perot, J., Nauleau, F., Moulin, P., 2010a. Application of magnetic nanoparticles for UF membrane integrity monitoring at low-pressure operation. J. Memb. Sci. 350, 172–179.
Guo, H., Wyart, Y., Perot, J., Nauleau, F., Moulin, P., Ce, P., 2010b. Low-pressure membrane integrity tests for drinking water treatment: a review. Water Res. 44, 41–57.
Henry, C., Brant, J.A., 2012. Mechanistic analysis of microfiltration membrane fouling by buckminsterfullerene (C60) nanoparticles. J. Memb. Sci. 415–416, 546–557.
Henry, C., Dorr, B., Brant, J.A., 2012. Buckminsterfullerene (C60) nanoparticle fouling of microfiltration membranes operated in a cross-flow configuration. Sep. Purif. Technol. 100, 30–43.
Heymann, D., 1996. Solubility of fullerenes C60 and C70 in Seven Normal alcohols and their deduced solubility in water. Fuller. Sci. Technol. 4, 543–544.
Hofmann, T., von der Kammer, F., 2009. Estimating the relevance of engineered carbonaceous nanoparticle facilitated transport of hydrophobic organic contaminants in porous media. Environ. Pollut. 157, 1117–1126.
Hong, S., Elimelech, M., 1997. Chemical and physical aspects of natural organic matter (NOM) fouling of nanofiltration membranes. J. Memb. Sci. 132, 159–181.
Howe, K.J., Marwah, A., Chiu, K.-P., Adham, S.S., 2007. Effect of membrane configuration on bench-scale MF and UF fouling experiments. Water Res. 41, 3842–3849.
Huang, H., Lee, N., Young, T., Gary, A., Lozier, J.C., Jacangelo, J.G., 2007. Natural organic matter fouling of low-pressure, hollow-fiber membranes: effects of NOM source and hydrodynamic conditions. Water Res. 41, 3823–3832.
Huang, H., Young, T., Jacangelo, J.G., 2008. Unified membrane fouling Index for low pressure membrane filtration of natural Waters: principles and Methodology. Environ. Sci. Technol. 42, 714–720.
Jafvert, C.T., Kulkarni, P.P., 2008. Buckminsterfullerene's (C60) octanol-water partition coefficient (Kow) and aqueous solubility. Environ. Sci. Technol. 42, 5945–5950.
Jassby, D., Chae, S.-R., Hendren, Z., Wiesner, M., 2010. Membrane filtration of fullerene nanoparticle suspensions: effects of derivatization, pressure, electrolyte species and concentration. J. Colloid Interface Sci. 346, 296–302.
Jung, Y.K., Kim, M.J., Kim, Y.-J., Kim, J.Y., 2013. Limitation of UV-Vis absorption analysis for determination of aqueous colloidal fullerene (nC60) at high ionic strength. KSCE J. Civ. Eng. 17, 51–59.
Kolkman, A., Emke, E., Bäuerlein, P.S., Carboni, A., Tran, D.T., ter Laak, T.L., van Wezel, A.P., de Voogt, P., 2013. Analysis of (functionalized) fullerenes in water samples by liquid chromatography coupled to high-resolution mass spectrometry. Anal. Chem. 85, 5867–5874.
Kroto, H.W., Heath, J.R., O'Brien, S.C., Curl, R.F., Smalley, R.E., 1985. C60: buckminsterfullerene. Nature 318, 162.
Ladner, D., Steele, M., Weir, A., Hristovski, K., Westerhoff, P., 2011. Functionalized nanoparticle interactions with polymeric membranes. J. Hazard. Mater 211–212, 288–295.
Li, D., Frey, M.W., Joo, Y.L., 2006. Characterization of nanofibrous membranes with capillary flow porometry. J. Memb. Sci. 286, 104–114.
Li, Y., Zhang, W., Zhang, X., Chen, C., Wang, J., 2010. Characterization of fouling in immersed polyvinylidene fluoride hollow fibre membrane ultrafiltration by particles and natural organic matter. Desalin. water Treat. 18, 2010.
Lohwacharin, J., Takizawa, S., 2009. Effects of nanoparticles on the ultrafiltration of surface water. J. Memb. Sci. 326, 354–362.
Lyon, D.Y., Adams, L.K., Falkner, J.C., Alvarezt, P.J.J., 2006. Antibacterial activity of fullerene water suspensions: effects of preparation method and particle size. Environ. Sci. Technol. 40, 4360–4366.
Montes-Burgos, I., Walczyk, D., Hole, P., Smith, J., Lynch, I., Dawson, K., 2010. Characterisation of nanoparticle size and state prior to nanotoxicological studies. J. Nanopart. Res. 12, 47–53.
Mulder, M., 1991. In: Basic Principles of Membrane Technology, Second Ed. Kluver Academic Publishers.
Murayama, H., Tomonoh, S., Alford, J., Karpuk, M.E., 2004. Fullerene production in tons and more: from science to industry. Fuller. Nanotub. Carbon Nanostruct. 12, 1–9.
Navarro, E., Baun, A., Behra, R., Hartmann, N.B., Filser, J., Miao, A.-J., Quigg, A., Santschi, P.H., Sigg, L., 2008. Environmental behavior and ecotoxicity of engineered nanoparticles to algae, plants, and fungi. Ecotoxicology 17, 372–386.
Osawa, E., 2002. Perspective of Fullerene Nanotechnology. Germany, Berlin.
van Oss, C.J., 2006. Interfacial forces in aqueous Media. In: Interfacial Forces in Aqueous Media, Second Edition, second ed. CRC Press.
Sayes, C.M., Gobin, A.M., Ausman, K.D., Mendez, J., West, J.L., Colvin, V.L., 2005. Nano-C60 cytotoxicity is due to lipid peroxidation. Biomaterials 26, 7587–7595.
Schafer, A.I., 2000. Microfiltration of colloids and natural organic matter. J. Memb. Sci. 171, 151–172.
Singh, R., 2015. Membrane Technology and Engineering for Water Purification. Elsevier.
Song, M., Yuan, S., Yin, J., Wang, X., Meng, Z., Wang, H., Jiang, G., 2012. Size-dependent toxicity of nano-C60 aggregates: more sensitive indication by apoptosis-related Bax translocation in cultured human cells. Environ. Sci. Technol. 46, 3457–3464.
Stone, V., Nowack, B., Baun, A., van den Brink, N., Kammer, F. Von Der, Dusinska, M., Handy, R., Hankin, S., Hassellöv, M., Joner, E., Fernandes, T.F., 2010. Nanomaterials for environmental studies: classification, reference material issues, and strategies for physico-chemical characterisation. Sci. Total Environ. 408, 1745–1754.
Tang, C.Y., Chong, T.H., Fane, A.G., 2011. Colloidal interactions and fouling of NF and RO membranes: a review. Adv. Colloid Interface Sci. 164, 126–143.
Tarabara, V.V., Hovinga, R.M., Wiesner, M.R., 2002. Constant transmembrane pressure vs. constant permeate flux: effect of particle size on crossflow membrane filtration. Environ. Eng. Sci. 19, 343–355.
Xie, Q.-L., Liu, J., Xu, X.-X., Han, G.-B., Xia, H.-P., He, X.-M., 2009. Size separation of Fe2O3 nanoparticles via membrane processing. Sep. Purif. Technol. 66, 148–152.
Yiantsios, S.G., Karabelas, A.J., 1998. The effect of colloid stability on membrane fouling. Desalination 9164, 143–152.
Zhu, S., Oberdorster, E., Haasch, M.L., 2006. Toxicity of an engineered nanoparticle (fullerene, C60) in two aquatic species, Daphnia and fathead minnow. Mar. Environ. Res. 62, 5–9.